

# Effects of Displacement Damage on the Time-Resolved Gain and Bandwidth of a Low Breakdown Voltage Si Avalanche Photodiode

Jamie S. Laird<sup>1</sup>, Shinobu Onoda<sup>2</sup>, Toshio Hirao<sup>2</sup>, Heidi Becker<sup>1</sup>, Allan Johnston<sup>1</sup> and Hisayoshi Itoh<sup>2</sup>

**Abstract—** Effects of displacement damage and ionization damage induced by gamma irradiation on the dark current and impulse response of a high-bandwidth low breakdown voltage Si Avalanche Photodiode has been investigated using picosecond laser microscopy. At doses as high as 10Mrad (Si) minimal alteration in the impulse response and bandwidth were observed. However, dark current measurements also performed with and without biased irradiation exhibit anomalously large damage factors for applied biases close to breakdown. The absence of any degradation in the impulse response is discussed as are possible mechanisms for higher dark current damage factors observed for biased irradiation.

## I. INTRODUCTION

Highly reliable Avalanche Photodiode's (APD) with reduced power requirements and improved temperature stabilization are a key device for high-speed low-light level applications where they can exhibit higher sensitivities than *p-i-n* structures if the gain-bandwidth product is high enough and the excess noise, low [1]. However, their response to radiation levels has been an issue of concern in recent years, particularly for use in space [2-5] and particle accelerator facilities [6]. Indeed, Hamamatsu now provides radiation hardened APD's for use as photodetectors in the CMS calorimeter of the large hadron collider at CERN [7-11].

Likewise, various space based astrophysical satellites are either using or are planning to in the near future, APD's for soft x-ray measurements [12-14] and free-space laser communications [15, 16]. These satellites, as well as devices close to the collision point in a high-energy physics experiment are susceptible to large fluence of high-energy particles which can introduce displacement damage (DD) at levels deleterious to bulk device parameters. Displacement damage from MeV electrons and protons are known to generate point defects responsible for an increase in the dark current and excess noise factor of Avalanche Photodiodes fabricated in Si [2, 3, 17] and InGaAs-InP [2, 4].

Beside an increase in dark current which obviously reduces the signal-to-noise ratio (increases the Noise Equivalent Power (NEP) by increasing shot noise, DD can also alter the effective doping level structure by either donor removal and/or acceptor compensation. In some instances,

radiation damage also leads to a reduction in the breakdown bias as observed in some Si [7] and InGaAs devices [4, 18]. Which devices fail and which survive appears to be a reliability issue probably due to dopant control in the near-surface region [8, 17].

Kirn et al. measured the spectral degradation in Si APD's with either SiO<sub>2</sub> or Si<sub>3</sub>N<sub>4</sub> passivation parameters subjected to <sup>60</sup>Co irradiation to levels up to 5.5MRad(S) [19]. These results were compared to those collected after neutron irradiation. In that work, ionization damage in the SiO<sub>2</sub> passivation layer was considerably worse than in Si<sub>3</sub>N<sub>4</sub> worse in the 300-600nm regime and marginally worse there above. No such degradation was noted in the neutron results leading to the conclusion that surface damage in passivation leads to a decrease in quantum efficiency, probably due to the incorporation of color centers.

Previous reports by Osborne et al [20] and Baccaro et al. [6] found neutron irradiation to levels around 10<sup>13</sup> n/cm<sup>2</sup> resulted in degradation in the gain. Similarly, simulations by Pilicer et al. for the Si APD variant used in the CMS calorimeter also indicate an alteration in the effective doping level  $N_{eff}$  with neutron fluence will eventually lead to some marginal degradation in gain, although little change was predicted for the wavelength dependence of the quantum efficiency [17]. Contrary to this, Antunovic et al. found no real degradation in the electrical characteristics beside the dark current for the radiation-hardening process employed by Hamamatsu [10]. However, these devices have a large area and wide junction, typically operating at around 380V (breakdown is at 450V). For use in space-craft APD's with similar gains and characteristics are desirable but with lower operating bias which simplifies support electronics saving space and probably reducing their own susceptibility to radiation effects. Having lower breakdown voltages requires the use of thinner junctions necessitating higher electric fields if similar gains are to be achieved. Although the work of Grahl et al. [7] have shown leakage to increase modestly in wider APD's, the higher electric fields in thinner junctions are likely to facilitate additional current generation mechanisms such as tunneling and Poole-Frenkel barrier reduction [21, 22].

Likewise, given the extreme sensitivity of gain with electric-field, it stands to reason that any changes in the effective doping are more likely to effect gain in thinner junction APD's. Since the APD examined in this work has transit-time limited performance, the impulse response and bandwidth (BW) of the device can in theory be affected. For high-frequency (HF) applications, any degradation in the gain (or bandwidth) of an APD can be critically determine

<sup>1</sup> California Institute of Technology (CALTEC), Jet Propulsion Laboratory (JPL), Pasadena, CA 91109, US  
email: Jamie.S.Laird@jpl.nasa.gov

<sup>2</sup> Department of Severe Environmental Materials, Japan Atomic Energy Agency (JAEA), Takasaki, Gunma, Japan  
email: Toshio.Hirao@jaea.go.jp

the Bit Error Rate (BER) for communications, and the signal-to-noise ratio (SNR) for more general applications [1].

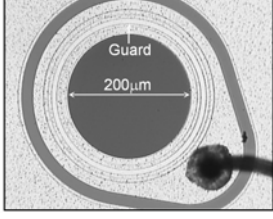


Figure 1: Photo of the 200 $\mu\text{m}$  Si APD indicating a possible guard structure around the edge as well as an isolating ring after which metallization is used to reduce diffusion currents. The ring structure is quite apparent in the scanned laser measurements shown later in Figure 5.

In this paper we examine the high-frequency gain of a low breakdown voltage Si APD subjected to  $^{60}\text{Co}$  irradiation. Although, DD effects on the dark current have been studied in the past, the effects, if any, of trapped Space-Charge on the electric-field profile and HF gain has not been. A picosecond laser microscope is used to collect spatially resolved impulse response data from which gain, bandwidth and gain uniformity prior to, and after irradiation, were investigated. Different spot sizes were used to examine the influence of high-injection (HI) and low-injection (LI) conditions on the measured gain for all doses. CW gain data supplied by the manufacturer has been used to account for pre-irradiation lot-to-lot variation in APD characteristics.

Dark current in devices biased during irradiation indicates degradation is more severe than that predicted by Non-Ionizing Energy Loss (NIEL) alone; particularly for higher electric fields where hot carrier damage and defect migration rates may be substantially higher. Most previous studies performed irradiation at zero bias. Here both are performed for the highest irradiation point. One important ramification is that unlike biased irradiation which appeared to behave linearly with NIEL, predicting degradation under bias is complex particularly if both ionization damage in the isolation oxide and enhanced recoil damage in high-fields are indeed the mechanism

## II. AVALANCHE PHOTODIODE

### A. APD Design

The device chosen for the following tests was a 200 $\mu\text{m}$  diameter Hamamatsu Si APD part number S2381 with a peak responsivity of 0.5A/W at  $\lambda=800\text{nm}$ . The device's -3dB cutoff frequency  $f_{-3\text{dB}}$  was stated at 1GHz. The excess noise factor at  $M_{\text{cw}}=100$  is about 4 [23]. In total 10 devices were examined spanning several lots. The mean breakdown bias  $V_{\text{br}}=152\text{V}$  with a  $\sigma_{\text{br}}=6.3\text{V}$  whereas the mean reverse bias for a  $M_{\text{cw}}$  gain of 100 is  $V_r=140$  with the same  $\sigma_{\text{br}}$ . All of the manufacturers' measurements were made at 298K. Although a  $\sigma_{\text{br}}$  value of 6V may not seem large; close to breakdown a 6V spread can result in wide distribution of gains. Some normalization process is required if all devices are to be reliably compared on the same judgment plane. Here, the manufacturers operating bias for achieving a continuous wave (CW) gain of  $M_{\text{cw}}=100$  at 800nm were used to

normalize gain comparisons. The dopant profile measured by 4-point spreading resistance measurements is shown on the right of Figure 1. The device has a reach-through structure as will become more apparent in both its CV and IV characteristics.

### B. Displacement Damage on Electrical Characteristics

The unity gain dark current in the APD is simply composed of a junction GR current combined with surface leakage and a diffusion current from any surrounding bulk. The total unity gain dark current is simply:

$$I_d^{\text{unity}} = \frac{en_i w_j A_j}{\tau_{g,\text{eff}}} + en_i s_g A_s + \frac{en_i^2 D_p A_j}{N_d L_{p,\text{eff}}} \quad (1)$$

where  $n_i$  is the intrinsic carrier density,  $e$  is the electronic charge,  $w_j$  is the total junction width,  $s_g$  is the surface recombination velocity at the interface in question,  $D_p$  is the minority carrier diffusivity in the bulk and  $N_d$  is the doping level of the bulk. Both  $\tau_{g,\text{eff}}$  and  $L_{p,\text{eff}}$  refer to the respective effective GR lifetime and minority carrier diffusion length in the bulk [21]. Junction GR currents are typically larger than diffusion components at room temperatures unless the diffusion length is very short. The quality or signal-to-noise ratio of APD is affected by the Noise Equivalent Power (NEP) which has a root mean square (RMS) given by:

$$I_{\text{rms}}^2 = 2eMI_d^{\text{unity}}\Delta f + \frac{4kT\Delta f}{R_j} \quad (2)$$

where  $R_j$  is the equivalent resistance of the PD and  $M$  is a gain. The first term is simply the shot noise from random fluctuations in carrier numbers, while the second is Johnson noise associated with thermal motion for a spectral bandwidth:

$$\Delta f = \int_0^{\infty} |H(f)|^2 df \quad (3)$$

where  $H(f)$  is the impulse response or transient photocurrent (TP) in this case [24]. By measuring the TP, the high frequency end of the BW can be extracted by inverse Fourier transform. At higher BW, the leakage current may begin to determine the overall Signal-to-Noise ratio (SNR). In the absence of parasitic elements, the -3dB BW  $f_{-3\text{dB}}$  of the APD is limited by the carrier transit-time combined with an extrinsic RC time constant  $f_{-3\text{dB}} = f_t^{-1} + f_{\text{RC}}^{-1}$  where  $f_t$  and  $f_{\text{RC}}$  are the respective transit and RC related -3dB BW points. Donor removal or acceptor compensation at high levels of DD result in changes in capacitance and series resistance which can shift the -3dB [25]. Changes in capacitance are also likely to have resulted in field and transit time elongation. High-speed devices of this nature have typical substrate densities of the order of  $10^{18}\text{cm}^{-3}$  to reduce series resistance and donor/acceptor compensation effects are minimal [25].

### C. APD High-Frequency Gain and Space-Charge Effects

For the laser wavelengths used here electrons generated in the near intrinsic region are transported into the  $M$ -region where they seed avalanche after traversing a finite path-length over some stochastic build-up time [26]. For Si

devices the ratio  $\alpha > \beta$  and noise can be minimized if electrons alone contribute to gain. The low frequency, continuous wave (CW) or DC gain  $M_{cw}$  for pure electron injection into a uniform  $E$ -field is simply:

$$M_{cw} = (\alpha - \beta) / (\alpha \exp[(\beta - \alpha)w_M] - \beta) \quad (2)$$

where  $\alpha$  and  $\beta$  are the electric-field dependent impact ionization coefficients for electrons and holes,  $w_M$  is the thickness of the  $M$ -region. In this work, the gain of interest is the high-frequency (HF) gain which is a more complicated function than its DC equivalent [26]. The expression typically used to formulate the HF gain has the form:

$$M_p(\omega) = M_{cw} / \sqrt{1 + \omega(M_{cw}t_{av} + t_t)^2} \quad (3)$$

where  $M_{cw}$  is the CW gain given by equation (2),  $\omega$  is the angular frequency,  $t_t$  is related to the mean transit time for carriers to cross the multiplication region and  $t_{av}$  is the avalanche build-up time [27] which has the same effect as an additional photo-capacitive  $RC$  time constant that compresses dynamic range thereby lowering  $f_{-3dB}$  [28]. According to Sze,  $M_p(\omega)$  reduces at higher frequencies due to series resistance and SC effects which reduces  $t_t$  [26] making it important to account for when measuring  $M_p$ . For all future references,  $M_{cw}$  will correspond to the CW or DC gain of the APD made by the manufacturer and  $M_p$  will refer to a pulsed or HF gain measurements.

#### D. High-Injection Effects on Gain

High-injection levels introduce a variety of phenomena which alter the spatiotemporal response of a device [29-33]. The most important of these being attributed to Space-Charge (SC) screening effects which perturb the  $E$ -field distribution resulting in an elongation of the transient photocurrent (TP) [31]. The influence of SC screening on the TP for three different injection levels  $\rho_1$ ,  $\rho_2$  and  $\rho_3$  is shown in Figure 2. A log scale best illustrates how the TP demarcates into two phases [32, 34, 35] denoted here as an ambipolar (perturbed  $E$ -field) and bipolar (unperturbed  $E$ -field) phase. The ambipolar and bipolar phases can be characterized by time-constants  $\tau_A$  and  $\tau_B$ , respectively [34]. HI levels screen the external field by inducing a dipolar field from the top to bottom edge of the plasma.

Carriers within the screened region diffuse via ambipolar diffusion until they reach the external field, after which they drift and are collected. As carrier levels reduce in time, a threshold level is crossed collapsing the dipolar field. Besides the small ambipolar field between them, carriers then drift *independent* (faster) bipolar carrier drift [32]. As the injection density  $\rho$  increases,  $\tau_A$  decreases, as noted in Figure 2. The  $B$ -phase parameter  $\tau_B$  is largely independent of injection level by definition. Since the transit time  $t_t$  in equation (6) is the sum of  $t_A$  and  $t_B$ , one can easily see that gain much necessarily decrease as injection levels are increased. Likewise the  $f_{-3dB}$  bandwidth must also decrease. According to Edmonds, an approximate 1-D expression relating the

charge collected in the  $A$ -phase to the location and density of an ion (or even laser) induced EHP plasma is simply:

$$Q_A(t) = \frac{D_n}{D_A} Q_0 G(D_A t / z_{max}^2) \quad (3)$$

where the function  $G$  is defined as:

$$G(\zeta) = 1 - \frac{8}{\pi^2} \sum_{n=0}^{\infty} (2n+1)^{-2} \exp[-(2n+1)^2 \pi^2 \zeta] \quad (4)$$

and  $z_{max}$  is the maximum depth of the carrier generation profile [36] which we approximate here as several absorption lengths. The term  $D_A$  is the ambipolar diffusivity which depends on injection condition. Under HI conditions the TP is dominated by the  $A$ -phase which predicts a sum of exponentials whose time-constants (the average of which is  $\tau_A$ ) depends on  $D_A$  and  $\alpha$ . Increased carrier-carrier scattering at higher injection leads to a decreasing  $D_A$  resulting in a slower decay [34].

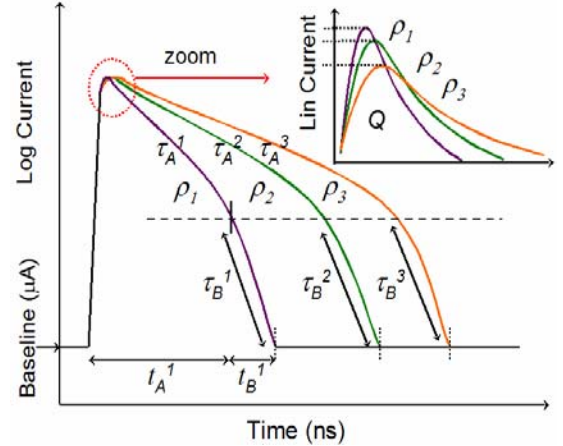


Figure 2: A diagram illustrating the influence of high-injection levels and SC effects on the TP for three increasing injection levels  $\rho_1 < \rho_2 < \rho_3$ , as displayed on a log and linear vertical scale (zoomed on the peak region). The ambipolar and bipolar phases can be characterized by time-constants  $\tau_A$  and  $\tau_B$ , respectively. With increasing  $\rho$ , the peak current decreases and  $\tau_A$  increases.

#### E. APD Irradiation

Displacement damage produced by gamma rays is an indirect process resulting from Compton electrons (with a 1.2MeV maximum energy). Si recoil energies are at most able to generate one or two displaced atoms per scattered electron [37].  $^{60}\text{Co}$  gamma irradiation was chosen due to its ease and simplicity with regards to maintaining an approximate room temperature during irradiation for all devices regardless of total dose and dose rate. The use of high biases for example would have required strict atmospheric and/or temperature control to limit the possibility of surface leakage or shorting due to condensation. All irradiations were performed at the Japan Atomic Energy Agency (JAEA), Takasaki, Japan. A total of five doses were performed on separate devices with exposures ranging over 10k, 100k 1M and 10M.

DUT	Dose (rad (Si))	$V_{br}$	$V_r (M_{cw}=100)$
1	10M	163	150.6
2	10M (biased)	151	138.4
3	1M	149	137.1
4	1M	157	144.7

5	100k	144	131.9
6	100k	154	142
7	10k	146	133.4
8	10k	159	147
9	0	145	133.2
10	0	152	140.5

Figure 3: Table assigning DUT number with measured  $V_{br}$ ,  $V_r$  for  $M_{cr}=100$  and dose applied to each device.

Dose rates of 150rad/s were used for all devices. All devices were irradiated in the dark with no electrical connections except one 10Mrad (Si) sample. According to Gill et al. *n*-Si material undergoes SCSI at around 90Mrad (Si), well above that examined here. Both of these devices were operated at a nominal high gain value of 125V to examine the issue of hot-carrier degradation, injection annealing [38] and *E*-field enhanced defect diffusion.

Not shown here are the Capacitance-Voltage (CV) measurements for the 0 to 40V range indicating statistically insignificant alteration with dose, including that of the biased irradiation. A range of 40V includes the pre-reach through region near the surface. Shown in Figure 4 are the set of dark current curves for the all doses illustrating a damage constant of for unbiased irradiation. Unlike the case of Becker et al.[2] where no bias was applied, here a typical application bias was applied for the maximum exposure which subsequently lead to a rapid degradation in the dark current. Interestingly, the dark current appears ohmic-like until breakdown, which remained at the same bias.

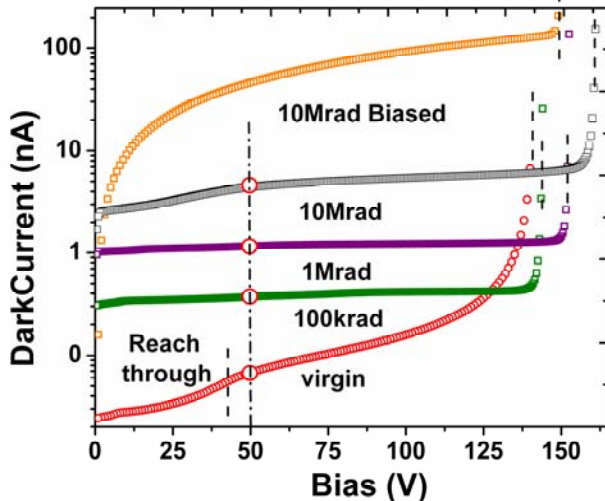


Figure 4: Dark current curves for the virgin (lowest) and all gamma irradiated devices. Also included is the biased device exposed to 10Mrad (Si) indicating a substantial degradation in leakage for biased irradiations.

#### F. Pulsed Laser Analysis on Virgin APD

A laser system incorporating a 788nm (close to DUT maximum response) picosecond laser diode (1.57eV) with a peak optical power of 167mW and Gaussian pulse shape of 46ps (FWHM) was used for the following  $M_p$  measurements. The laser was collimated, circularized, passed through a neutral density filter and steered via mirrors through an optical port into a chamber where an aspherical objective focuses the beam onto a temperature controlled DUT stage. All photodiodes were mounted on  $Al_2O_3$  double-ended

micro-stripline chip carriers with the  $p^+$  signal traversing a 50 $\Omega$  40GHz transmission line and bias tee before being acquired on the scope. The base was 50 $\Omega$  terminated. For larger leakage currents the internal drop across the bias tee resistance of 50 $\Omega$  needs to be considered. However, here maximum currents are fractions of micro-amps and losses are negligible. Here biases are limited to -15V (maximum bias across the 40GHz bias tee). Chip carriers are mounted on a liquid  $N_2$  cryostage designed for low-temperature analysis. Here the temperature was PID held at 300K. The modulation period  $t_m$  of the laser diode output was set at 10 $\mu$ s i.e. the modulation rate  $f_m$  is 1MHz. The number of pulses required to build an average waveform is high. This was deemed appropriate for examining high-frequency operation where even higher modulation rates are typically applied. However, given that most deep levels in irradiated Si have times constant of the order of microseconds, trap filling is expected to be high in the quasi-steady state (to be discussed later).

#### G. APD Gain Uniformity

A measurement of device gain under quasi low-injection condition whereby the entire APD is exposed to the laser assumes gain is uniformity is high. After focusing the beam close to the centre of the device, APD uniformity was examined for biases covering the complete range of operation using Transient Laser Beam Induced Current (LBIC). Scans of 500 $\mu$ m $\times$ 500 $\mu$ m were made across the device and parameters such as the peak current and charge were extracted from the measured impulse response at each position to form images. Shown in Figure 5 below is the peak current image of the APD at low (50V) and high-gain (100V) operation. The ring around the structure is the isolation spacing between the inner electrode and outer Al anti-diffusion mask as seen in the photo. At higher bias some non-uniformity appears around the inner edge as expected, comprising some 25% or so of the total volume available for impact ionization. Furthermore, Transient LBIC mapping of the 10Mrad biased device 2 was also carried out to examine degradation effects on the spatial uniformity of the high-injection gain. As seen in the 3<sup>rd</sup> image, there has been little changed after the 10Mrad (Si) irradiation besides a possible increasing of the edge region into the centre and an obvious decrease in the amplitude of the outer ring, probably due to a decreased minority carrier lifetime.

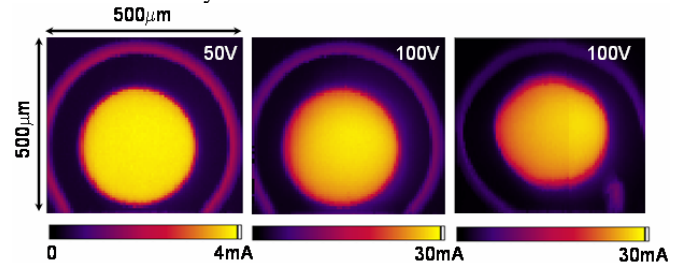


Figure 5: Transient LBIC peak current image of the virgin APD in low-gain (50V left) and high-gain (100V middle) modes. Non-uniformity in the 100V image probably introduces a small error into the  $M_p$  measurement. After a 10Mrad biased irradiation the image changes little except possible increase in the edge region instability and thickness, plus a decrease in the outer ring current due to the reduced minority carrier lifetime. The small lump at the bottom right is a reflection from the wirebond.

### H. APD Injection Dependent Gain Measurements

Measuring the injection dependence of the gain used the same technique for focusing. Initially an LBIC scan with the laser in CW mode was used to find an approximate centre of the DUT. Scanning in Z (the distance between the aspheric lens and DUT) was used to monitor the global minimum in the peak of the impulse response, which coincides with the highest injection point, and by corollary, the focal condition [39]. For the following scans, a Z range of  $\pm 2.5\text{mm}$  covers spot sizes from focus to well beyond the DUT diameter of  $200\mu\text{m}$  through to the focused spot size. This value was used to estimate  $M_p$  for all spot sizes up to the device diameter where the charge peak occurs as indicated by the symmetric peak positions as shown in Figure 6. The gain (positive after the reach-through bias of around 40V) assumes the unity gain charge is  $1.2\text{pC}$  as measured on a  $p-i-n$  structure. The HI (top circles) and LI (bottom squares) gains have been plotted in Figure 7.

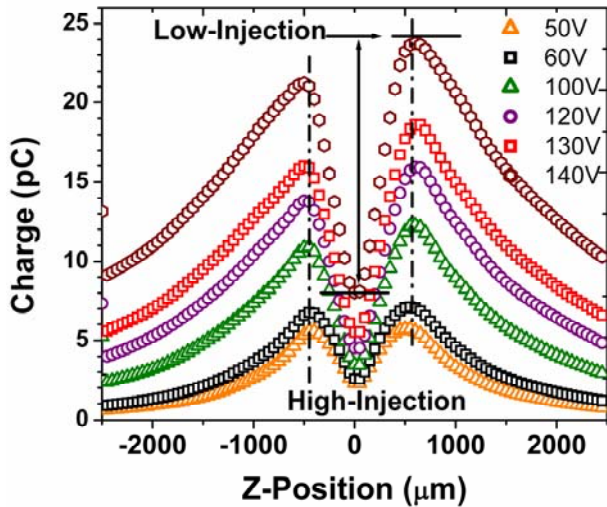


Figure 6: Charge collected by integrating the measured impulse response as a function of DUT to aspheric lens distance, Z. Increasing gain at higher biases has an obvious injection dependence as noted by the ratio in the Z=0 to t gain.

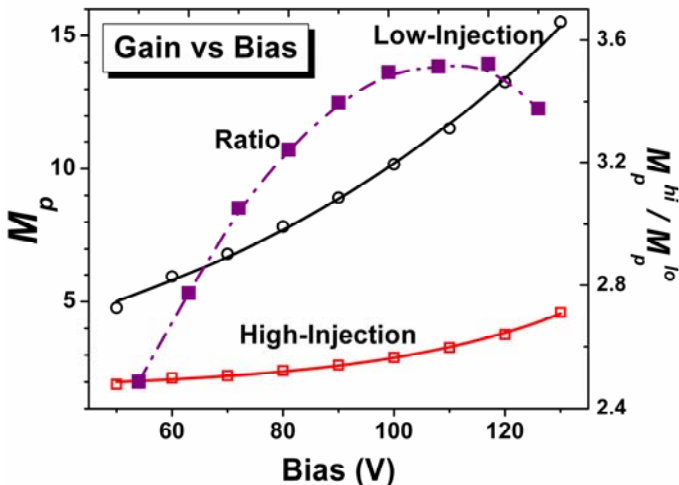


Figure 7: The pulsed gain  $M_p$  of the virgin DUT under low and high-injection conditions specified in Figure 6. Also shown on the right of the figure (solid squares) is the ratio of the two indicating SC effects degrade the gain until around 110-120V after which it begins to improve again.

Exponential fitting (solid line) to each curve returned excellent agreement. The fitted function was then used to extract  $M_p$  for the bias at which  $M_{cw}=100$ , as taken from Table 1. First of all, injection dependence aside, all values are significantly less than  $M_{cw}$  as predicted. Interestingly, in HI mode the relative increase in gain with increasing bias decreases as noted by the increasing ratio  $M_p^{hi}/M_p^{lo}$  which quantifies the increased dip height as a fraction of the maximum gain. As the gain is extremely sensitive to the E-field and the available path-length, small disturbance in either, result in large decreases. For biases greater than 100V, the ratio decreases indicating that more rapid plasma erosion is beginning to restore the field to its near steady state, or as close as it can be under quasi-LO injection.

### I. APD Gain on Irradiated Devices

The same procedure outlined on the virgin DUT was carried out on the entire range of irradiated devices. Likewise, the LO and HI gain were calculated for the bias  $V_r$  giving a pre-irradiation gain  $M_{cw}$  of 100 for each specific device was estimated using the method already outlined. Quite surprisingly, both the LO and HI gain did not change up to beyond 10Mrad including the biased device where dark current degradation was exacerbated by high-electric fields. Shown in Figure 9 are the normalized TP response for both the virgin and 10Mrad (Si) biased device under HI and LI conditions ( $Z=0\mu\text{m}$  and  $500\mu\text{m}$ , respectively). Not shown for brevity is TP data for the unbiased 10Mrad (Si) data taken at the same conditions. It data basically lies on the same two clearly demarcated branches separating the HI and LI conditions. The pre-irradiated risetime  $\tau_r$  of 200ps is essentially unchanged with DD, as is the falltime. Hence the -3dB BW of the device is also unchanged.

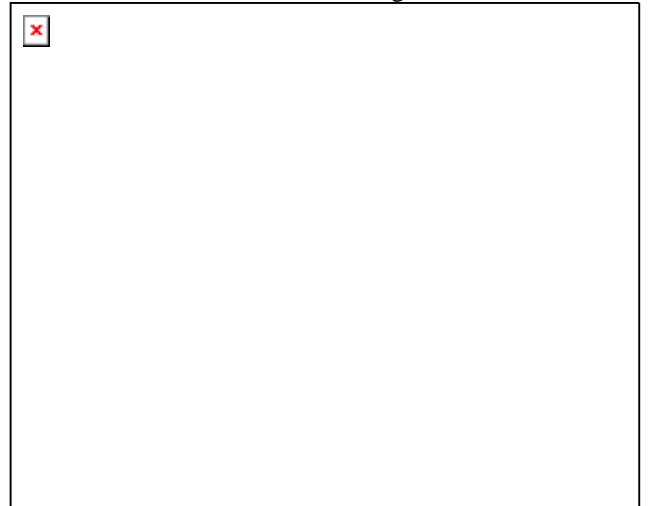


Figure 8: Calculated values of  $M_p^{lo}$  and  $M_p^{hi}$  vs. TD extracted from exponential fits to the gain-bias curves similar to that presented in Figure 7. Very little change with TD is noted up until 10Mrad. Both the biased and unbiased irradiation had little impact on the HF gain.

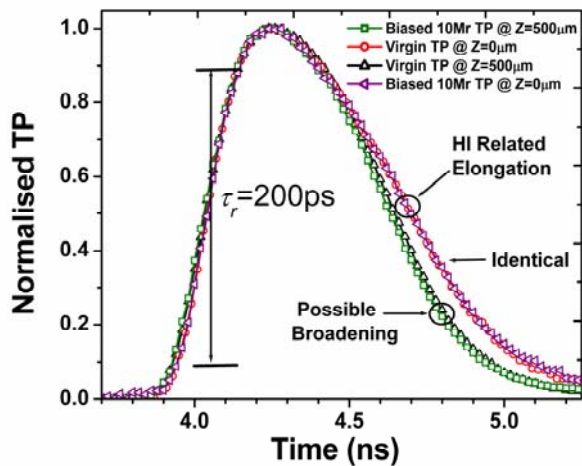


Figure 9: Normalized transient photocurrents at 100V for both HI ( $Z=0\mu\text{m}$ ) and LI ( $Z=500\mu\text{m}$ ) conditions measured on the virgin and 10Mrad(Si) device irradiated under bias. Beside the tail elongation under HI conditions there is surprisingly no change in pulse shape and BW after irradiation.

### III. DISCUSSION

#### A. Dark Current Degradation

Dark current degradation under no applied bias changes very little with bias beyond the reach-through bias of approximately 40V. In fact, using the measured Mp curves with bias for the 1Mrad(Si)

#### B. Anomalous Dark Current Degradation

This may be explained by the fact that for the same gain ( $M_{cw}=100$ ), the considerably lower operating biases for this APD necessarily implies a much thinner junction and higher  $E$ -field. Hot-carriers and charged atoms liberated by Compton electrons are likely to be further heated resulting in higher point defect introduction rates. Moreover, the higher electric-field in this thin device is likely to not only separate charged defects thereby reducing the possibility of self-annealing from spatiotemporally overlapping defects [40] but also posit remaining defects closer to the high and low-field regions i.e. near the surface and substrate interface. A high number of defects in the high-field region is likely to result in additional tunneling current, coupled defect interaction [41], and Frenkel-Poole barrier lowering which decreases the activation energy, increasing the SRH generation current [42]. The Frenkel-Poole effect does of course require a charged centre after trap capture. Srour et al. has in previous displacement damage studies on CCD arrays observed activation energies exhibiting all of the above [22, 43].

To calculate the damage constant for the irradiation series two points are now compared. The damage constant used here is that based on the displacement damage dose (DDD) introduced by Walters et al and used by Srour to describe displacement damage in Si devices [42]. A bias of 50V was chosen since the gain is close to unity and small differences in APD characteristics will not result in gross change in gain and errors in estimating the damage constant,  $\alpha$ . The field is not high enough to substantially increase the DDD of the

primary Compton electron i.e. only keV acceleration can occur representing less than a 0.1% increase in energy. However, any displaced atoms which are charged and can be accelerated to produce further damage; possibly cascades if enough energy can be built up. Mobile charged defects in Si are also known to drift in a high enough electric fields [44]. Since the Compton electron energy is of the order of an MeV, accelerating it by a modest keV or so in the high field region is unlikely to increase the energy it imparts to Si recoils. Furthermore, the electrons ejected with a significant velocity component in the direction of the field will also be a small fraction of the total.

The rapid rise for low applied bias may be due to a range of causes: (a) donor removal and compensation related extension of the SC region volumetrically increased the number of traps contributing to GR at low biases, (b) the field profile has altered close to the surface causing enhanced emission rates from Poole-Frenkel lowering or tunneling and (c) defects have either migrated there under the applied field or additional defects were generated in the first place, (d) ionization damage and possible extension of in the surrounding isolation oxide forming the guard ring and (e) bias dependent annealing. However, case (b) is likely to be negligible as noted by no change in the low injection gain after irradiation. Likewise, the need for a low series resistance as noted by the dopant profile and the lack of change in responsivity with dose (it should decrease with increasing series resistance if the doping is low to moderate), means the GR volume cannot increase by the amount required to account for a three orders magnitude increase in leakage. Furthermore, the decreased field would reduce enhanced emission and reduce GR currents near the surface. No such decrease in the  $E$ -field has already been implied by the unchanging peak response. Indeed, the epitaxial structure with a low-resistivity substrate is intrinsically hard [45].

#### 1) Charged Recoil Multiplication

The difference may also lie in the fact that during defect generation more defects are in fact being generated. For gamma irradiation, typical Si recoils possess 150eV as opposed to several keV for neutron induced displacements [Li reference]. These lower energies typically displace one or two atoms [37]. If these low energy recoils are charged, their acceleration in the high fields may in fact lead to further recoils. If the mean-free path is long enough, higher energy recoils may lead to possible clustering, or at least defect levels where electron wave-functions may overlap leading to coupled defect behavior. Both possibilities will definitely lead to considerably higher dark currents [46] due to processes already outlined for high electric fields and the addition now of coupled-defect interactions which leads to better “traffic flow” between bands and higher GR rates [41]. Insignificant change in the CV profile after irradiation with bias tends to suggest...

#### 2) Ionization Damage in the Guard Isolation Oxide

The GUARD structure used here reduces the field around the edge by stepping it down across several rings whose total distance is probably greater than the fully depleted thickness. Although EDGE breakdown cannot occur, leakage current around the edges are added to that of the APD center. According to Becker et al. ionization damage is also a key concern for Si APD's [3]. By comparing proton and  $^{60}\text{Co}$  irradiation Becker et al. concluded ionization damage in the isolation oxide can generate additional leakage. The frequency dependence of noise measurements indicated strong  $1/f$  components further indicative of surface states being to blame [47]. For biased operation performed here the situation becomes worse; especially if the field is in the direction of the substrate [47]. During the biased irradiation ionization due to the Compton electrons in the  $E$ -field of the isolation oxide drifts electrons and hole in opposite directions, reducing the chance for geminate recombination [47]. The higher mobility of electrons sweeps them to the contact where they are collected. Holes on the other hand have a low mobility in  $\text{SiO}_2$  and trap at defects deep in the oxide. Electrons tunneling across the interface recombine with holes that make it close to the interface. The interface trap density at the surface  $D_{it}$  reduces the surface recombination lifetime  $\tau_s$  resulting in a large increase in the GR current. The effective generation lifetime approaches that due to surface recombination when  $\tau_s \gg \tau_g$  as is probably the case here if surface leakage is indeed responsible for much of the dark current [21]. As the guard structure is not separate, any increase in dark current at the guard is added in parallel to the center but not gained. Any lateral expansion of the parasitic MOS inversion layer should be observable in differences between the CV characteristics of the biased versus unbiased irradiation. Unfortunately, the metallization doesn't allow the increased charge collection volume to be mapped with the laser.

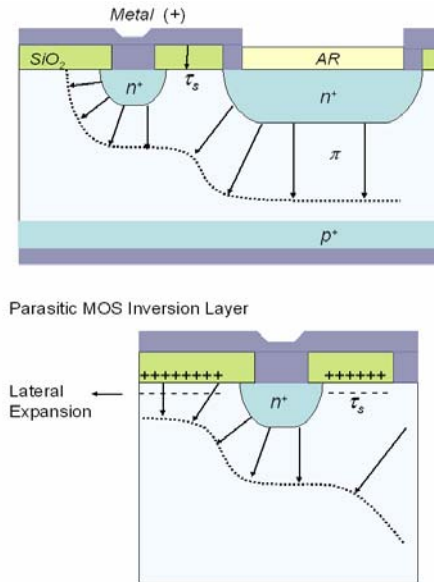


Figure 10: Diagram of the basic guard structure around the APD to reduce pre-mature breakdown at the edge of the  $n^+$  implant as indicated by the equipotential and  $E$ -field lines. After irradiation, ionization in the oxide leads to hole trapping and interface traps at the interface. This leads to an inversion layer which dramatically reduces the surface recombination lifetime,  $\tau_s$ .

### 3) Bias Dependent Annealing

Bias-dependent radiation annealing has been observed by Cindro et al. and Mikuz et al. in high-resistivity  $n$ -Si diodes irradiated with neutrons and heavy ions [48, 49]. Biased annealing rates were found to be considerably lower, as monitored by a significant increase in the full depletion voltage. For this case, self-annealing at the slightly elevated temperature present during irradiation, which is itself much longer than typical particle irradiation, means biased annealing can play a significant role on short-term and long term annealing pathways. However, switching off the bias mid-anneal resulted in eventual restoration of the depletion voltage over longer periods. The conclusion drawn was that biased operation tends to inhibit short-term annealing even during long-term anneals with the bias applied. The  $E$ -field appears to retard the annealing rate of a particular defect. However, no systematic difference existed between the dark current with and without bias, meaning the defect was likely far from mid-gap. Fengmei et al. observed differences in defect formation due to neutron, electron and gamma irradiated biased detectors using Deep level Transient Spectroscopy (DLTS) [Fengmei et al. See Cindro paper].

#### C. Time-Resolved Gain Fluence Dependence

The HF gain under low and high-injection appears to alter very little with TD levels up to 10Mrad (Si) indicating (a) no issues with ionization damage in passivation/anti-reflection layers, (b) no alteration in the effective doping throughout the structure since there are no losses due to series resistance and changes in of the substrate and (b) minimal alteration in the  $E$ -field profile. The lack of any decrease in the quantum efficiency, even up to 10Mrad (Si), makes it highly probable that the passivation is  $\text{Si}_3\text{N}_4$ .

With regards to (b), given SC effects were shown to hugely impact the local field at relatively LI levels, we can only assume that traps are having little effect on the local SC density. A quantity termed the filling factor  $F$  defines the probability that a trap is occupied for a position  $E_t$  below  $E_c$ :

$$F = n_t / (N_t - n_t)$$

The situation is self-restoring in some ways; higher biases where field changes should lead to gain degradation also happens to be where leakage is highest and trap saturation heaviest. At room temperature leakage currents are large enough to provide sufficient carriers to fill traps. Traps are probably neutral after carrier capture leading to negligible change in the effective doping level,  $N_{eff}$ . In Figure 11 below, the influence of a modulated laser strike on the effective doping density is illustrated for three different modulation rates,  $f_m$ . When the modulation rate is greater than the trap emission rate, trapped charge builds up thereby altering  $N_{eff}$ . The other thing is the electric field profile is kind of frozen into place by the low-resistivity of the substrate as noted in no change in the responsivity.

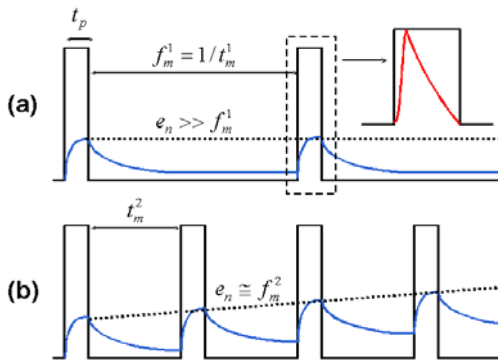


Figure 11: Carrier-capture detrapping balance for a modulated pulsed laser. The measured signal approaches that of the asymptotic TP which depends on the balanced trap populations and its influence of charge collection.

For single photon or low light level applications the situation could worsen especially at lower temperatures where laser injected carriers determine trap filling factors [Li]. Ideally a low modulation rate would be used and time-dependent trapping studies would be required to build a more complete picture. Another paper examining the low-temperature response of MeV electron irradiated *p-i-n* structures examines these issues in more detail [Laird].

#### IV. CONCLUSION

#### V. ACKNOWLEDGEMENTS

#### VI. REFERENCES

- [1] S. Donati, *Photodetectors: Devices, Circuits and Applications*. New Jersey: Prentice Hall, 2000.
- [2] H. N. Becker, "Dark Current Degradation of Near Infrared Avalanche Photodiodes from Proton Irradiation," *IEEE Transactions on Nuclear Science*, 2004.
- [3] H. N. Becker, *et al.*, "The influence of structural characteristics on the response of silicon avalanche photodiodes to proton irradiation," *Nuclear Science, IEEE Transactions on*, vol. 50, pp. 1974-1981, 2003.
- [4] J. S. Laird, *et al.*, "Heavy-ion induced single-event transients in high-speed InP-InGaAs avalanche photodiodes," *IEEE Transactions on Nuclear Science*, vol. 50, pp. 2225-2232, 2003.
- [5] J. S. Laird, "High-Injection Related Transient Anomalous Gain Mechanisms in Avalanche Photodiodes Studied With Focused MeV Ions," *Journal of Applied Physics*, vol. To Be Submitted Feb 2005, 2005.
- [6] S. Baccaro, *et al.*, "Radiation damage effect on avalanche photodiodes," *Nuclear Instruments and Methods in Physics Research Section A: Accelerators, Spectrometers, Detectors and Associated Equipment*, vol. 426, pp. 206-211, 1999.
- [7] J. Grahl, *et al.*, "Radiation hard avalanche photodiodes for CMS ECAL," *Nuclear Instruments and Methods in Physics Research Section A: Accelerators, Spectrometers, Detectors and Associated Equipment*, vol. 504, pp. 44-47, 2003.
- [8] D. Bailleux, *et al.*, "Hamamatsu APD for CMS ECAL: quality insurance," *Nuclear Instruments and Methods in Physics Research Section A: Accelerators, Spectrometers, Detectors and Associated Equipment*, vol. 518, pp. 622-625, 2004.
- [9] A. Accotto, *et al.*, "A study of symmetrical LLL X-ray polyolithic interferometers on the basis of the Takagi equations," *Zeitschrift-fur-Physik-B-(Condensed-Matter)*, vol. 95, pp. 151-65, 1994.
- [10] Z. Antunovic, *et al.*, "Radiation hard avalanche photodiodes for the CMS detector," *Nuclear Instruments and Methods in Physics Research Section A: Accelerators, Spectrometers, Detectors and Associated Equipment*, vol. 537, pp. 379-382, 2005.
- [11] Z. Antunovic, *et al.*, "Uniformity measurements across the area of the CMS ECAL avalanche photodiodes," *Nuclear Instruments and Methods in Physics Research Section A: Accelerators, Spectrometers, Detectors and Associated Equipment*, vol. 545, pp. 139-144, 2005.
- [12] J. Kataoka, *et al.*, "Recent progress of avalanche photodiodes in high-resolution X-rays and Gamm rays detection," *Nuclear Instruments and Methods in Physics Research Section A: Accelerators, Spectrometers, Detectors and Associated Equipment*, vol. Submitted, 2004.
- [13] S. Kishimoto, "High time resolution x-ray measurements with an avalanche photodiode detector," presented at Proceedings of the 4th international conference on synchrotron radiation instrumentation, 1992.
- [14] J. R. Palmer, *et al.*, "The use of avalanche photodiodes for the detection of soft x rays," presented at Proceedings of the 4th international conference on synchrotron radiation instrumentation, 1992.
- [15] D. L. Begley, *Free Space Laser Communications II*, vol. MS-100: SPIE Optical Engineering Press, 1994.
- [16] R. M. Gagliardi, *et al.*, *Optical Communications*. New York: John Wiley and Sons, 1976.
- [17] E. Pilicer, *et al.*, "Excess noise factor of neutron-irradiated silicon avalanche photodiodes," *Nuclear Instruments and Methods in Physics Research Section A: Accelerators, Spectrometers, Detectors and Associated Equipment*, vol. 552, pp. 146-151, 2005.
- [18] J. S. Laird, *et al.*, "Non-linear charge collection mechanisms in high-speed communication avalanche photodiodes," *Nuclear Instruments and Methods in Physics Research Section A: Accelerators, Spectrometers, Detectors and Associated Equipment*, vol. 541, pp. 228-235, 2005.
- [19] T. Kirn, *et al.*, "Wavelength dependence of avalanche photodiode (APD) parameters," *Nuclear Instruments and Methods in Physics Research Section A: Accelerators, Spectrometers, Detectors and Associated Equipment*, vol. 387, pp. 202-204, 1997.
- [20] M. D. Osborne, *et al.*, "Numerical simulation of neutron radiation effects in avalanche photodiodes," *Electron Devices, IEEE Transactions on*, vol. 47, pp. 529-536, 2000.
- [21] D. K. Schroder, "Carrier Lifetimes in Silicon," *IEEE Transaction on Electron Devices*, vol. 44, pp. 160-179, 1997.
- [22] J. R. Srouf, *et al.*, "Enhanced displacement damage effectiveness in irradiated silicon devices," 1989.
- [23] Hamamatsu-Corporation, "Application Notes / User Manual," 2000.
- [24] J. C. Campbell, "Photodetectors for Long-Wavelength Lightwave Systems," in *Semiconductor Lasers Sources and Photodetectors*, J. C. Campbell, Ed.
- [25] J. S. Laird, *et al.*, "Irradiation Induced Degradation of High-Speed Response of Si PIN photodiodes Studied by Pulsed Laser Measurements," *IEEE Transactions on Nuclear Science*, vol. 50, pp. 2003-2010, 2003.
- [26] S. M. Sze, *Physics of Semiconductor Devices*. New York: J.Wiley, 1981.
- [27] G. Lucovsky, *et al.*, "Transit-Time Considerations in p-i-n Diodes," *Journal of Applied Physics*, vol. 35, pp. 5-12, 1965.
- [28] K. J. Williams, *et al.*, "Photodiode compression due to current-dependent capacitance," *International Topical Meeting on Microwave Photonics*, pp. 221-224, 2000.
- [29] P. A. Tove, *et al.*, "Recombination in light-pulse excited silicon at medium-high carrier concentration levels," *Journal of Applied Physics*, vol. 44, pp. 2690-2692, 1973.
- [30] K. J. Williams, "Design Considerations for High-Current Photodetectors," *IEEE Journal of Lightwave Technology*, vol. 17, 1999.
- [31] K. J. Williams, *et al.*, "Non-Linearities in p-i-n Microwave Photodetectors," *IEEE Photonics Technology Letters*, vol. 14, 1996.
- [32] J. S. Laird, *et al.*, "High-injection carrier dynamics generated by MeV heavy ions impacting high-speed photodetectors," *Journal of Applied Physics*, vol. 98, pp. 013530, 2005.

- [33] F. Hieronymi, *et al.*, "Influence of Space Charges on the Impulse Response of Metal-Semiconductor-Metal Photodetectors," *IEEE Journal of Lightwave Technology*, vol. 10, 1992.
- [34] S. Tiwari, *et al.*, "On the role of mobility and saturated velocity in the dynamic operation of p-i-n and metal-semiconductor-metal photodetectors," *Applied Physics Letters*, vol. 60, pp. 1135-1137, 1992.
- [35] P. A. Tove, *et al.*, "Plasma Effects in Semiconductor Detectors," *Nuclear Instruments and Methods in Physics Research*, vol. 51, pp. 261-269, 1967.
- [36] L. D. Edmonds, "Charge Collection from Ion Tracks in Simple Epi Diodes," *IEEE Transactions on Nuclear Science*, vol. 44, pp. 1448, 1997.
- [37] H. C. Julius, "Irradiation Damage in Germanium and Silicon due to Electrons and Gamma Rays," *Journal of Applied Physics*, vol. 30, pp. 1310-1316, 1959.
- [38] R. J. Walters, *et al.*, "Radiation response and injection annealing of p/sup +/n InGaP solar cells," *Solid-State-Electronics*, vol. 42, pp. 1747-56, 1998.
- [39] J. S. Laird, *et al.*, "A Novel Method for Optimizing the Focus of an Ultrafast Photon Source Using the Transient Photocurrent of a High-Speed Device," *Measurement Science and Technology*, vol. 17, pp. 789-796, 2006.
- [40] A. Hallen, *et al.*, "The influence of ion flux on defect production in MeV proton-irradiated silicon," *Journal of Applied Physics*, vol. 70, pp. 3025-3030, 1991.
- [41] A. Schenk, *et al.*, "Coupled Defect Level Recombination: Theory and Application to Anomalous Diode Characteristics," *Journal of Applied Physics*, vol. 77, 1995.
- [42] J. R. Srour, *et al.*, "Universal damage factor for radiation-induced dark current in silicon devices," 2000.
- [43] J. R. Srour, "Displacement Damage Effects in Electronic Materials, Devices and Integrated Circuits," in *NSREC Short Course*, D. G. Platteter, Ed.: IEEE, 1988.
- [44] R. G. Elliman, *et al.*, "Single-energy, MeV implant isolation of multilayer III-V device structures," *Journal of Applied Physics*, vol. 71, pp. 1010-1013, 1992.
- [45] Z. Li, *et al.*, "Investigation of epitaxial silicon layers as a material for radiation hardened silicon detectors," 1997.
- [46] K. Gill, *et al.*, "Bulk Damage Effects in Irradiated Silicon Detectors due to clustered divacancies," *Journal of Applied Physics*, vol. 82, pp. 126-136, 1997.
- [47] T. P. Ma, *et al.*, *Ionizing Radiation Effects in MOS Devices and Circuits*: Wiley Interscience, 1989.
- [48] V. Cindro, *et al.*, "Bias-dependent radiation damage in high-resistivity silicon diodes irradiated with heavy charged particles," *Nuclear Instruments and Methods in Physics Research Section A: Accelerators, Spectrometers, Detectors and Associated Equipment*, vol. 450, pp. 288-296, 2000.
- [49] M. Mikuz, *et al.*, "Bias dependence and bistability of radiation defects in silicon," *Nuclear Instruments and Methods in Physics Research Section A: Accelerators, Spectrometers, Detectors and Associated Equipment*, vol. 466, pp. 345-353, 2001.